Toughened carbon nanotube-iron-mullite composites prepared by spark plasma sintering

Alicia Weibel, Alain Peigney, Geoffroy Chevallier, Claude Estournès, Christophe Laurent

Toughened carbon nanotube–iron–mullite composites prepared by spark plasma sintering

Alicia Weibel, Alain Peigney, Geoffroy Chevallier, Claude Estournès, Christophe Laurent*

Université de Toulouse, Institut Carnot CIRIMAT, UPS CNRS, Université Paul-Sabatier, 118 Route de Narbonne, 31062 Toulouse Cedex 9, France

Abstract

Carbon nanotube–iron–mullite nanocomposite powders were prepared by a direct method involving a reduction in H_2–CH_4 and without any mechanical mixing step. The carbon nanotubes are mostly double- and few-walled (3–6 walls). Some carbon nanofibers are also observed. The materials were consolidated by spark plasma sintering. Their electrical conductivity is 2.4 S/cm whereas pure mullite is insulating. There is no increase in fracture strength, but the SENB toughness is twice than the one for unreinforced mullite (3.3 vs. 1.6 MPa $m^{1/2}$). The mechanisms of carbon nanotube bundle pullout and large-scale crack-bridging have been evidenced.

Keywords: A. Spark plasma sintering; B. Nanocomposites; D. Mullite; D. Carbon nanotubes

1. Introduction

Carbon nanotubes (CNTs) show a high aspect ratio and excellent mechanical, electrical and thermal properties. For example, a Young's modulus close to 1 TPa [1] and a tensile strength up to 60 GPa [2] have been reported. For multi-walled CNTS (MWCNTs), an electrical conductivity higher than 10^5 S/m [3] and a thermal conductivity higher than 3000 W/mK [4] have been reported. Therefore, ceramic–matrix composites containing CNTs have been increasingly studied for about fifteen years as revealed by recent reviews of the field [5,6]. In particular, toughening is intensively researched. It is important to note that the presence of CNTs induces changes in the kinetics and mechanisms of sintering [7], which can greatly modify the matrix microstructure [8] and may in turn have a greater effect on the properties than the actual presence of CNTs [9,10]. Mullite is the name of some Al_2O_3–SiO_2 compounds. The most widely studied form is $Al_6Si_2O_{13}$ (also commonly designated $3Al_2O_3{:}2SiO_2$), an important material for electronic, optical and high-temperature structural applications, which are however limited by a low toughness [11]. Nevertheless, CNT–mullite composites are seldom studied. Wang et al. [12] prepared such materials by mixing powders of multi-walled CNTs (MWCNTs), Al_2O_3 and SiO_2, followed by hot-pressing in argon. These authors reported a moderate increase in bending strength and a strong increase in toughness, compared with pure mullite. Fracture of MWNTs and pullout of MWNTs at interfaces were proposed as reinforcement mechanisms. In the present work, CNT–Fe–mullite composites are prepared by an *in situ* catalytic chemical vapor deposition (CCVD) route [13], without any mixing or milling, thus avoiding any damage to the CNTs at this step. The powders are consolidated by spark plasma sintering (SPS), which requires lower temperatures and shorter times than hot-pressing. The mechanical properties and electrical conductivity are investigated.

2. Material and methods

2.1. Powder synthesis

The synthesis of the mullite and CNT–Fe–mullite composite powders was reported elsewhere [13]. Mullite ($Al_6Si_2O_{13}$) and iron-substituted mullite ($Fe_{0.6}Al_{5.4}Si_2O_{13}$) powders were prepared by a combustion method. The required proportions of $Al(NO_3)_3 \cdot 9H_2O$, $Fe(NO_3)_3 \cdot 9H_2O$ and NH_4NO_3 (5/6 of

*Corresponding author. Tel.: +33 5 61 55 61 22; fax: +33 5 61 55 61 63.

E-mail address: laurent@chimie.ups-tlse.fr (C. Laurent).

the molar quantity of the metal nitrates) were dissolved in an aqueous suspension of colloidal SiO_2, using the minimum amount of water. The required proportion of urea (the fuel) was added under continuous stirring up to complete dissolution. The urea proportion was double than the one necessary to reach the so-called stoichiometric ratio calculated from the total oxidizing valence of the nitrates and the reducing valence of urea [14]. The dish containing the mixture was placed in a furnace preheated at 600 °C, keeping the door of the furnace open. After water evaporation, a combustion reaction takes place between the nitrates and urea, thus producing an oxide powder. The as-prepared mullite powder was calcined in air at 1200 °C and the as-prepared $Fe_{0.6}Al_{5.4}Si_2O_{13}$ powder was divided into two batches, which were calcined in air at 1000 and 1100 °C, respectively (heating rate 300 °C/h, 1 h dwell, natural cooling), producing powders with a different specific surface areas (4.5 and 2.6 m^2/g, respectively). The so-obtained $Fe_{0.6}Al_{5.4}Si_2O_{13}$ powders were CCVD treated in H_2–CH_4 (20 mol% CH_4, maximum temperature 1050 °C, no dwell, heating and cooling rates 300 °C/h), in order to prepare the CNT–Fe–mullite composite powders. The flowing gas was dried on P_2O_5. Its composition and flow (15 L/min) were monitored using massflow controllers. The so-obtained powders are designated C1000R and C1100R hereafter.

2.2. Spark plasma sintering

The powders were consolidated by SPS (Dr Sinter 2080, SPS Syntex Inc., Japan). Samples were loaded into a 20 mm inner-diameter graphite die. A sheet of graphitic paper was placed between the punch and the powder as well as between the die and the powder for easy removal. The powders were sintered under vacuum (residual cell pressure < 3 Pa). A pulse configuration of 12 pulses (one pulse duration 3.3 ms) followed by 2 periods (6.6 ms) of zero current was used. Heating rates of 150 °C/min and 100 °C/min were used from room temperature to 600 °C and from 600 to 1500 °C, respectively. A 5 min dwell was applied at 1500 °C. An optical pyrometer, focused on a little hole at the surface of the die, was used to measure the temperature. A uniaxial load (corresponding to a uniaxial pressure of 150 MPa) was applied from 600 °C upwards and maintained during the dwell. Natural cooling was applied down to room temperature. The uniaxial pressure was gradually released during cooling. The final sintered specimens were in the form of pellets 20 mm in diameter and 2 mm thick.

2.3. Characterization

The carbon content in the powders was determined by flash combustion with a relative accuracy of 2%. The specific surface area was measured by the BET method using N_2 adsorption at liquid-N_2 temperature (Micromeritics FlowSorb II 2300). The reproducibility of the results is $\pm 3\%$. The sintered pellets were polished with a diamond paste up to 1 μm. The density of the pellets was measured by the Archimedes method. X-ray diffraction (XRD) patterns were recorded using a Bruker D4 Endeavor diffractrometer equipped with a Cu K_α radiation tube. The powders and sintered specimens were observed by field-emission-gun scanning electron microscopy (FESEM,

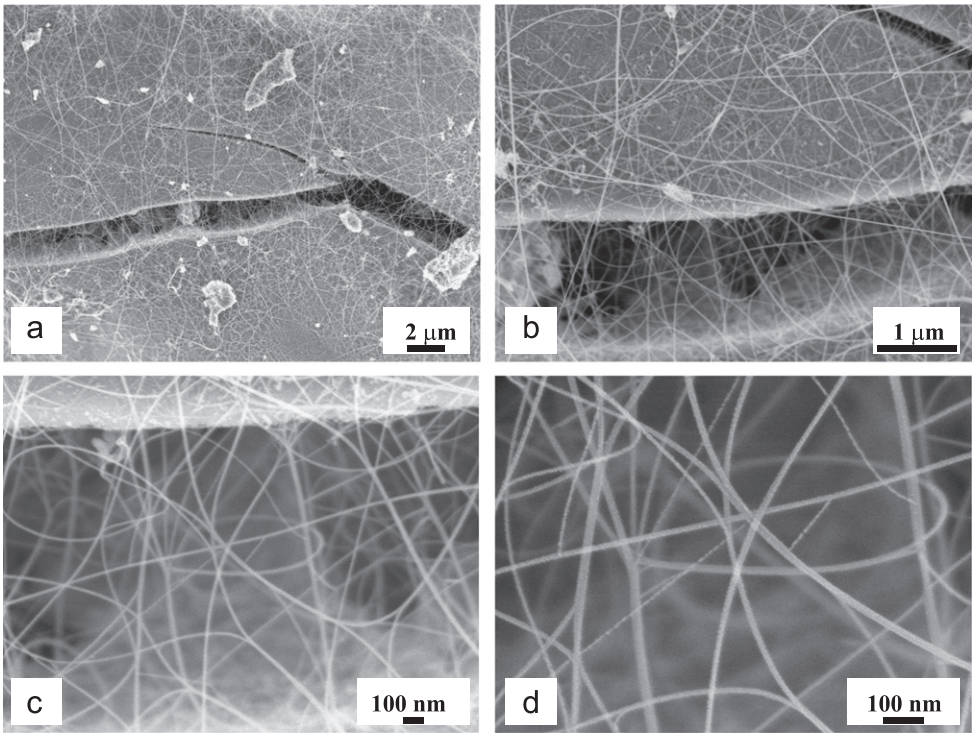

Fig. 1. FESEM images (at an increasing magnification of the same area) of the C1000R CNT–Fe–mullite powder.

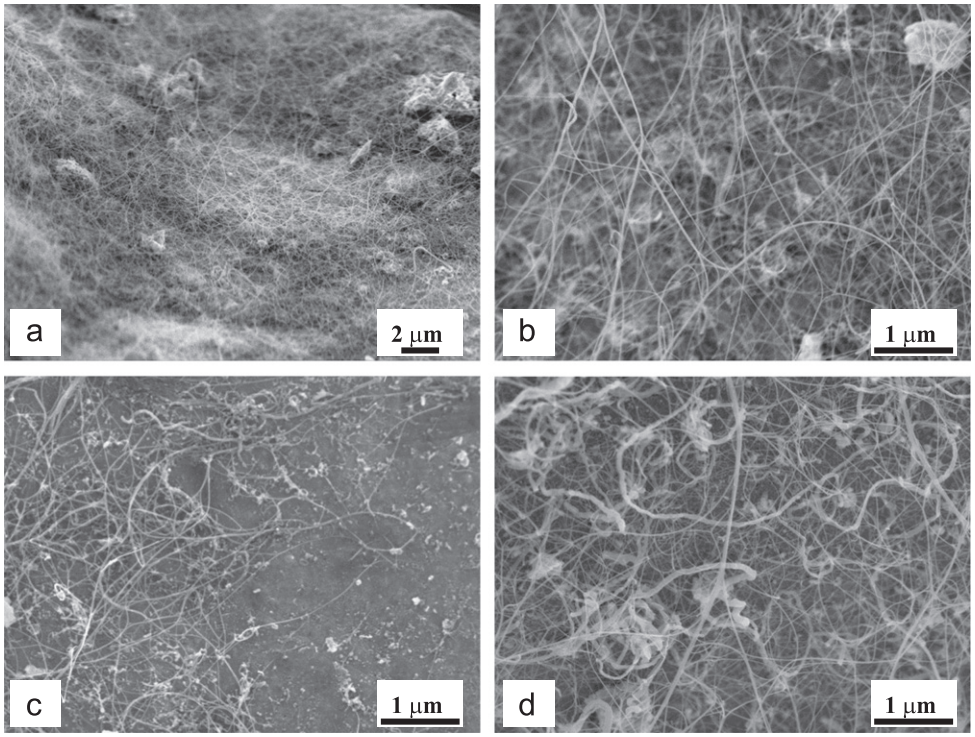

Fig. 2. FESEM images of the C1100R CNT–Fe–mullite powder.

JEOL JSM 6700F). The electrical conductivity was measured at room temperature with d.c. currents on parallelepipedic specimens ($1.6 \times 1.6 \times 8\ mm^3$), parallel to their length, *i.e.* perpendicular to the pressing axis. The current densities used were lower than 160 mA/cm^2 (Keithley 2400). The indentation tests were performed (5 N for 10 s in air at room temperature) on the polished surface of the specimens by loading with a Vickers indenter (Shimadzu HMV 2000). The corresponding diagonals of the indentation were measured using an optical microscope attached to the indenter. The fracture strength was measured by the three-point bending method on specimens about $1.6 \times 1.6 \times 18\ mm^3$ machined with a diamond saw. Cross-head speed was fixed at 0.1 mm/min. The toughness (K_{Ic}) was calculated from three-point bending results on notched specimens (single-edge notch beam, SENB) using a calibration factor [15]. A notch slightly less than half the thickness of the specimen was made using a 100 μm diameter SiC wire.

3. Results and discussion

3.1. Powders

The formation of the CNT–Fe–mullite powders (C1000R and C1100R) by the CCVD treatment of $Fe_{0.6}Al_{5.4}Si_2O_{13}$ was studied in detail elsewhere [13]. The composition and microstructure of the powders are fairly complex. Indeed, corundum (α-Al_2O_3), hercynite ($FeAl_2O_4$) and α-Fe peaks are detected on the XRD patterns in addition to mullite peaks. Moreover, analysis of ^{57}Fe Mössbauer spectra revealed that γ-Fe/C (a γ-Fe phase alloyed with carbon) and Fe_3C (cementite) are also present but in quantities small enough to remain undetected by XRD. Indeed, the proportions of α-Fe, γ-Fe/C and Fe_3C (about 40, 5 and 10% of all iron phases, respectively) show that slightly more than half the iron ions have been reduced. Thus, the content of reduced phases (α-Fe, γ-Fe/C and Fe_3C) in the material is

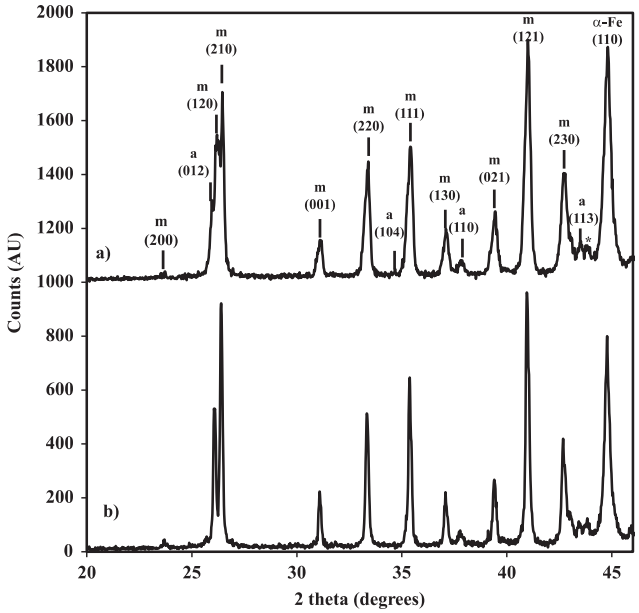

Fig. 3. XRD patterns of the C1000RS (a) and C1100RS (b) CNT–Fe–mullite specimens prepared by SPS. m: mullite; a: α-Al_2O_3; *: unidentified peak.

Table 1
Characteristics and properties of the materials prepared by SPS. C_n: carbon content; ρ: density; HV: Vickers microhardness, σ_f: fracture strength; K_{Ic}: SENB toughness; σ: electrical conductivity.

	C_n (wt%)	ρ (g cm^{-3})	HV (GPa)	σ_f (MPa)	K_{Ic} (MPa m$^{1/2}$)	σ (S/cm)
Mullite	0	3.09	15.1	238	1.6	–[a]
C1000RS	2.2	3.20	14.2	248	3.3	2.4
C1100RS	3.0	3.16	13.5	240	2.8	2.4

[a]The electrical conductivity of the mullite pellet is lower than 10^{-13} S/cm but cannot be given with precision, because the measured resistance value was the detection limit of the equipment.

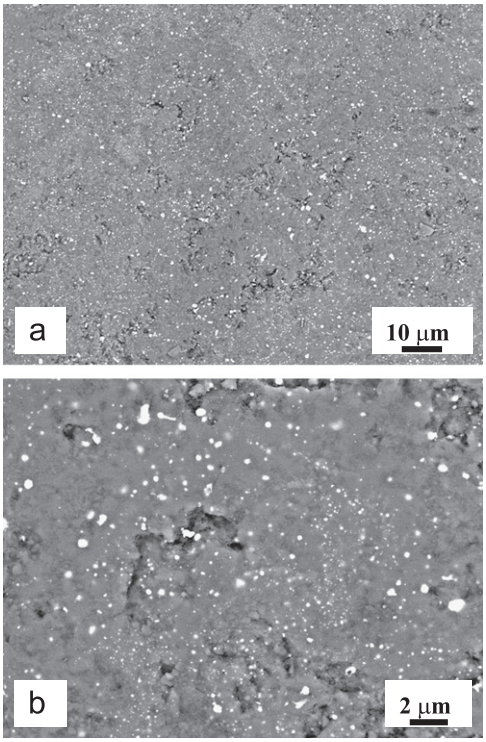

Fig. 4. Typical FESEM images (back-scattered electron images in chemical contrast mode) of the polished surface of the C1000RS CNT–Fe–mullite specimen. C1100RS is similar.

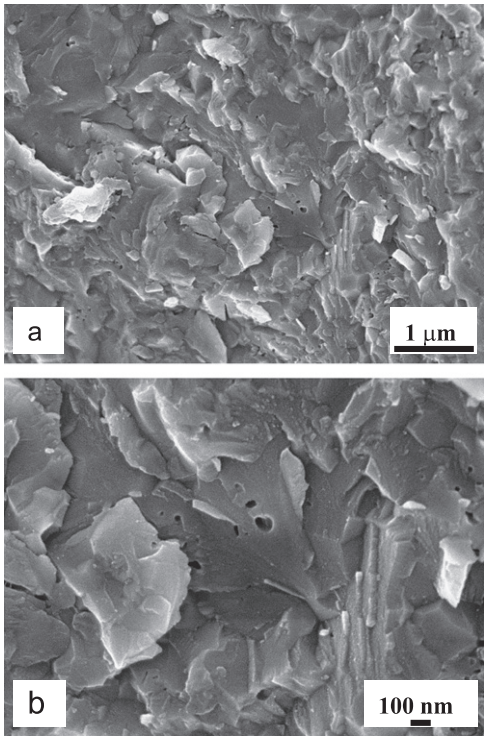

Fig. 5. Typical FESEM images of the fracture surface of the mullite specimen.

estimated to be about 4 wt%. The carbon content in the C1000R and C1100R powders is 2.3 and 3.0 wt%, respectively. The specific surface areas are similar to each other (6.1 and 6.2 m^2/g, respectively). These values are slightly higher than those found for the corresponding catalytic materials. As pointed out earlier [16], the deposition of carbon in the composite powder, notably in the form of CNTs, is responsible for most of this additional surface area. Low-magnification FESEM images [13] revealed that the mullite grains, several tens of micrometers in size, are fairly irregularly shaped. High-magnification FESEM images of C1000R (Fig. 1) and C1100R (Fig. 2) show long and flexible filaments homogeneously covering the surface of the mullite grains (Figs. 1a, b and 2a). The surface of the filaments is smooth and regular, their diameter is lower than 30 nm and their length is of the order of a few tens of micrometers (Fig. 1b–d). From earlier results, it is known that such filaments are isolated CNTs and/or CNTs bundles. For both powders, but more so for C1100R, some grains are covered by a mixture of CNTs and carbon nanofibers, which are easily detectable because their surface is rough and their diameter is in the range 30–80 nm (Fig. 2b–d). High-resolution transmission electron microscopy images [13] revealed that the CNTs are mostly double-walled and few-walled (3–6 walls).

3.2. Sintered specimens

Analysis of the XRD patterns of the composite pellets (Fig. 3) reveals that mullite is the major oxide phase, whereas the peaks for corundum are less intense than for the corresponding powders. No hercynite is detected, showing that the totality of hercynite and part of corundum have been dissolved into mullite upon the increase in temperature up to 1500 °C during SPS. The (110) α-Fe peak is more intense and narrower than it was for the

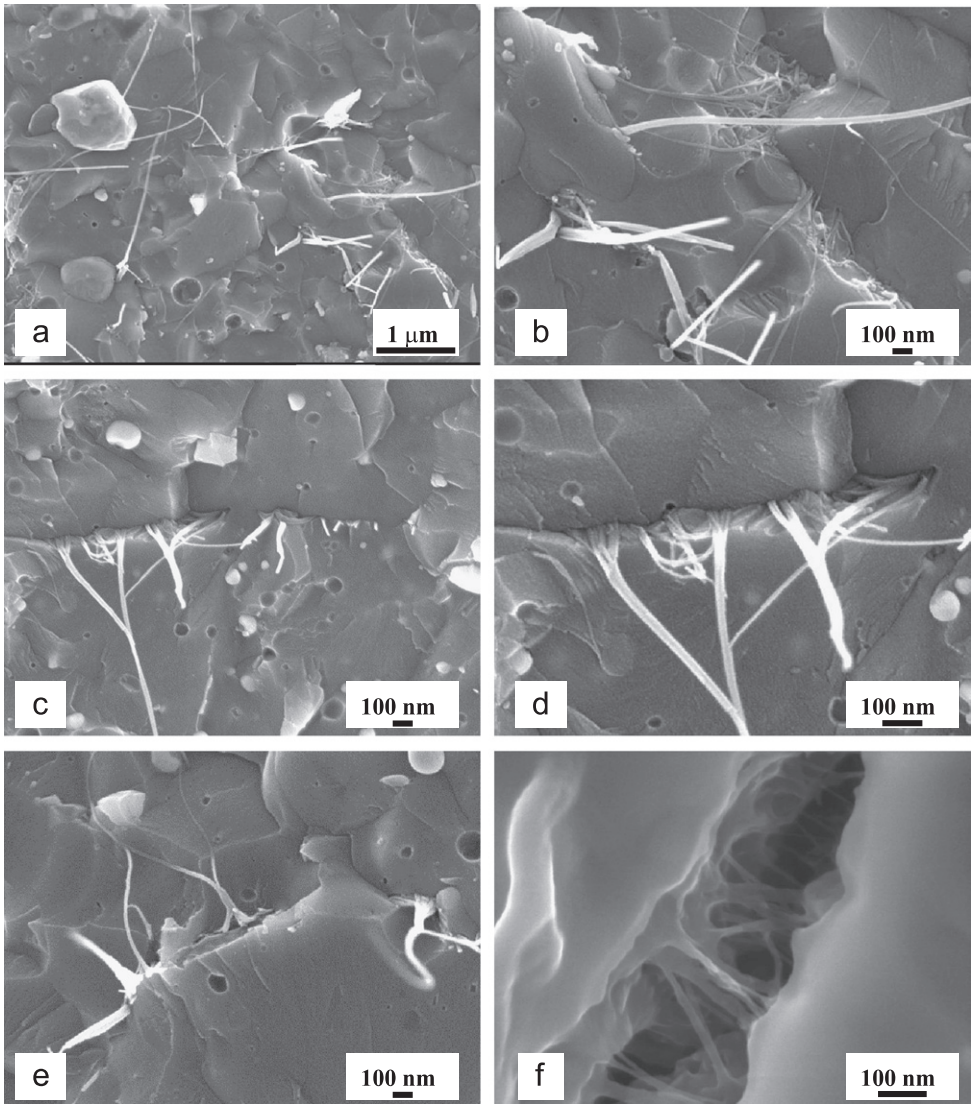

Fig. 6. Typical FESEM images of the fracture surface of the CNT–Fe–mullite specimens.

powders, reflecting the growth of the Fe crystallites. The density evaluated by the Archimedes method is equal to 3.09, 3.21 and 3.16 for the mullite, C1000RS and C1100RS specimens, respectively. The relative density is difficult to calculate because there is too much uncertainty on the actual composition of the materials. The electrical conductivity, Vickers microhardness, fracture strength and toughness are reported in Table 1. The electrical conductivity of the mullite pellet is lower than 10^{-13} S/cm but cannot be given with precision, because the measured resistance value was the detection limit of the equipment. For both C1000RS and C1100RS, the electrical conductivity is 2.4 ± 0.2 S/cm, which could indicate that the CNTs are mostly undamaged using the present SPS conditions, as confirmed by FESEM observations presented later in this study. The Vickers microhardness of C1000RS (14.2 GPa) and C1100RS (13.5 GPa) are lower than that of mullite (15.1 GPa). The fracture strength values for pure mullite and both composites (about 240 MPa) are lower than the values reported by Wang et al. [12] for pure mullite and a 3 wt% CNT–mullite composite (384 and 432 MPa, respectively) prepared by hot-pressing at the same temperature than our samples (1500 °C) and reported to have reached full density. Note that the measured densities were not reported in [12] and therefore it is difficult to compare with the present data. For mullite, it is reported [12] that fracture strength is increased when increasing the hot-pressing temperature to 1600 and 1650 °C (466 and 443 MPa, respectively). For the composites, fracture strength is increased when increasing the hot-pressing temperature to 1600 °C (512 MPa) despite achieving a lower relative density (96%) whereas it is markedly lower (302 MPa) upon a further increase to 1650 °C, which is thought [12] to reflect a still lower relative density ($< 94\%$) and fewer numbers of pullout MWNTs. This could in turn reflect that the CNTs were damaged upon hot-pressing at 1650 °C. Indeed, comparing hot-pressing and SPS revealed that the former technique cause much more damage to the CNTS, possibly because of the longer times

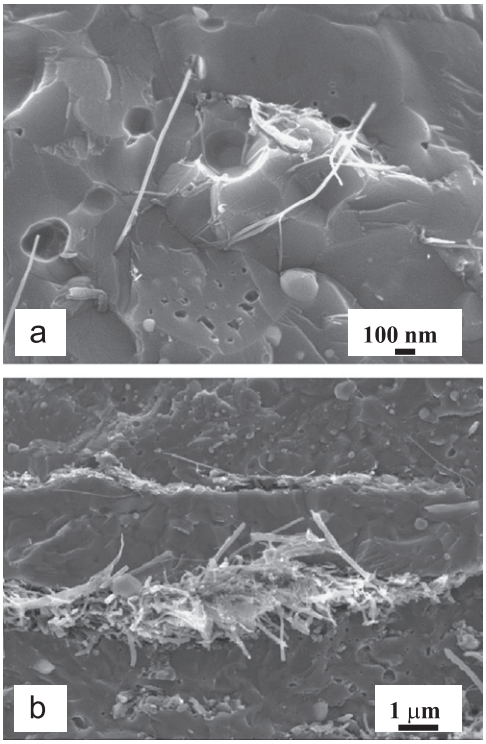

Fig. 7. Typical FESEM images of the fracture surface of the C1000RS and C1100RS CNT–Fe–mullite specimens showing undesirable carbon nanofibers (a) and bundles agglomerates at the grain boundaries (b).

involved [7,17]. The toughness for C1000RS (3.3 MPa $m^{1/2}$) is significantly higher than the values reported [12] for pure mullite and a 3 wt% CNT–mullite composite hot-pressed at 1500 °C (1.72 and 2.91 MPa $m^{1/2}$, respectively). It is similar to the values reported for the composites hot-pressed at 1550 and 1600 °C (3.27 and 3.60 MPa $m^{1/2}$, respectively). For C1100RS, the toughness (2.8 MPa $m^{1/2}$) is lower than for C1000RS, which could be due to the presence of carbon nanofibers. FESEM images (back-scattered electron images in chemical contrast mode) of the polished surface of C1000RS (Fig. 4) show the presence of some residual porosity, which could contribute to the low fracture strength. The Fe particles (appearing as white dots in the images) are fairly homogeneously dispersed and their diameter is in the range about 50 nm to 1 μm, most of them being however smaller than 200 nm. C1100RS (images not shown) is very similar to C1000RS. The possible role of the Fe particles on the mechanical properties is fairly complex. Indeed, it was proposed that a low Fe content favors strengthening whereas a high Fe content favors a moderate toughening [18]. This warrants further studies. FESEM images of the fracture surface of mullite (Fig. 5) and the composites (Fig. 6) show that the fracture is mostly transgranular although some intergranular fracture is also observed. Some residual porosity is observed in all specimens. Note however that round holes such as those observed in Fig. 6c are the original locations of Fe particles that happened to remain on the other (unobserved) side of the fracture. The CNTs appear to be undamaged. Some CNT bundles are cut near the matrix grain surface but some are protruding from the surface, suggesting some degree of bundle pullout (Fig. 6a). CNT bundles emerging from the matrix grain boundaries are also observed (Fig. 6b–e). Interestingly, large-scale crack-bridging is observed (Fig. 6f) in a crack about 300–500 nm wide, as shown in earlier studies on DWCNT–Al_2O_3 [6] and DWCNT–MgO composites [19]. Most CNTs appear to be taught, *i.e.* under tensile stress. It is thus probable that they directly contribute to the reinforcement. Carbon nanofibers (Fig. 7a) and excessive amounts of bundles agglomerated at the grain boundaries (Fig. 7b) are also observed. The latter could act as cracks and limit the cohesion and strength of the matrix grain boundaries. However, this is not widespread in the material, as evidenced by the mainly transgranular fracture mode, and could probably be avoided if the $Fe_{0.6}Al_{5.4}Si_2O_{13}$ powders were ball-milled or attrition-milled in order to decrease the grain size, prior to the reduction step. This would favor a better distribution of the CNTs around the mullite grains when they are formed *in situ* during the CCVD treatment.

4. Conclusions

The SENB toughness of a CNT–Fe–mullite nanocomposite consolidated by SPS is twice than the one for unreinforced mullite (3.3 vs. 1.6 MPa $m^{1/2}$). The mechanisms of crack-bridging by the CNTs and CNT bundle pullout have been evidenced. The electrical conductivity of the nanocomposites is 2.4 S/cm whereas mullite is insulating. The CNTs, mostly double- and few-walled (3–6 walls), appear to be undamaged and are fairly homogeneously dispersed at the mullite grain boundaries. These results arise because of the unique microstructure achieved through the use of an *in situ* route obviating any milling step for the synthesis of composite powders and through consolidation by SPS. However, carbon nanofibers and bundles agglomerated at the grain boundaries are also observed in some areas and weaken the materials. Therefore, reducing the matrix grain size to obtain a better CNT dispersion will be the subject of future work. The possible role of the Fe particles on the mechanical properties also warrants further studies.

Acknowledgments

SPS was performed at the Plateforme Nationale CNRS de Frittage-Flash (PNF^2, Toulouse). FESEM was performed at TEMSCAN, the "Service Commun de Microscopie Electronique", Université Paul-Sabatier.

References

[1] M.M.J. Treacy, T.W. Ebbesen, J.M. Gibson, Exceptionally high Young's modulus observed for individual carbon nanotubes, Nature 381 (1996) 678–680.

[2] M.F. Yu, O. Lourie, M.J. Dyer, K. Moloni, T.F. Kelly, R.S. Ruoff, Strength and breaking mechanism of multiwalled carbon nanotubes under tensile load, Science 287 (2000) 637–640.
[3] Y. Ando, X. Zhao, H. Shimoyama, G. Sakai, K. Kaneto, Physical properties of multiwalled carbon nanotubes, International Journal of Inorganic Materials 1 (1999) 77–82.
[4] M.J. Biercuk, M.C. Llaguno, M. Radosavlijevic, J.K. Hyun, A.T. Johnson, Carbon nanotube composites for thermal management, Applied Physics Letters 80 (2002) 2767–2769.
[5] J. Cho, A.R. Boccaccini, M.S.P. Shaffer, Ceramic matrix composites containing carbon nanotubes, Journal of Materials Science 44 (2009) 1934–1951.
[6] E. Zapata-Solvas, D. Gomez-Garcia, A. Dominguez-Rodriguez, Towards physical properties tailoring of carbon nanotubes-reinforced ceramic matrix composites, Journal of European Ceramic Society 32 (2012) 3001–3020.
[7] A. Peigney, S. Rul, F. Lefèvre-Schlick, Ch. Laurent, Densification during hot-pressing of carbon nanotube–metal–magnesium aluminate spinel nanocomposites, Journal of European Ceramic Society 27 (2007) 2183–2193.
[8] E. Flahaut, A. Peigney, Ch. Laurent, Ch. Marlière, F. Chastel, A. Rousset, Carbon nanotube–metal-oxide nanocomposites: microstructure, electrical conductivity and mechanical properties, Acta Materialia 48 (2000) 3803–3812.
[9] W.A. Curtin, B.W. Sheldon, CNT-reinforced ceramics and metals, Materials Today 7 (2004) 44–49.
[10] A. Kasperski, A. Weibel, C. Estournès, Ch. Laurent, A. Peigney, Preparation–microstructure–property relationships in double-walled carbon nanotubes/alumina composites, Carbon, 53 (2013) 62–72.
[11] H. Schneider, J. Schreuer, B. Hildmann, Structure and properties of mullite—review, Journal of European Ceramic Society 28 (2008) 329–344.
[12] J. Wang, H. Kou, X. Liu, Y. Pan, J. Guo, Reinforcement of mullite matrix with multi-walled carbon nanotubes, Ceramics International 33 (2007) 719–722.
[13] V.G. de Resende, Xu Hui, Ch. Laurent, A. Weibel, E. De Grave, A. Peigney, Fe-substituted mullite powders for the *in-situ* synthesis of carbon nanotubes by catalytic chemical vapor deposition, Journal of Physical Chemistry C 113 (2009) 11239–11245.
[14] K.C. Patil, Advanced ceramics combustion synthesis and properties, Bulletin of Materials Science 16 (1993) 533–541.
[15] W.F. Brown, J.E. Srawley, Plane strain crack toughness testing of high strength metallic materials, ASTM Special Technical Publication, American Society for Testing and Materials, Philadelphia, 1966, p. 410.
[16] A. Peigney, Ch. Laurent, F. Dobigeon, A. Rousset, Carbon nanotubes grown *in-situ* by a novel catalytic method, Journal of Materials Research 12 (1997) 613–615.
[17] F. Legorreta Garcia, C. Estournès, A. Peigney, A. Weibel, E. Flahaut, Ch. Laurent, Carbon nanotube-magnesia nanocomposites by spark-plasma-sintering: microstructure, electrical conductivity and microhardness, Scripta Materialia 60 (2009) 741–744.
[18] H. Wang, T. Sekino, T. Kusunose, T. Nakayama, K. Niihara, Properties and microstructure of mullite-based iron nanocomposite, Key Engineering Materials 317–318 (2006) 611–614.
[19] A. Peigney, F. Legorreta Garcia, C. Estournès, A. Weibel, Ch. Laurent, Toughening and hardening in double-walled carbon nanotube/nanostructured magnesia composites, Carbon 48 (2010) 1952–1960.